In-situ monitoring using ATR-SEIRAS of the electrocatalytic reduction of CO_2 on Au in an ionic liquid / water mixture

*Marco Papasizza and Angel Cuesta**

Department of Chemistry, School of Natural and Computing Sciences, University of Aberdeen, AB24 3UE Aberdeen, Scotland, UK.

ABSTRACT. The electrochemical reduction of CO_2 to CO in ionic liquids and ionic-liquid / water mixtures has received considerable attention due to recent claims of extraordinarily high energy efficiencies. We report here a study of CO_2 electroreduction on Au in a [EMIM]BF_4 / H_2O mixture (18% mol / mol) combining cyclic voltammetry and surface-enhanced infrared absorption spectroscopy in the attenuated total reflection mode (ATR-SEIRAS). The onset of the reduction current in the CV coincides with a decrease of the interfacial CO_2 concentration, but the appearance of adsorbed CO (CO_{ad}) is slightly delayed, as CO must probably first reach a minimum concentration at the interface. Comparisons with spectra collected in the absence of CO_2 and in CO-saturated electrolyte reveal that the structure of the double layer at negative potentials is different when CO_2 is present (probably due to the formation of CO_{ad}) and allow us to assign the main band in the spectra to CO adsorbed linearly on Au (CO_L), with a smaller band corresponding to bridge-bonded CO (CO_B). The CO bands show a large inhomogeneous broadening and are considerably broader than those typically observed in aqueous electrolytes. While both CO_L and CO_B can be observed in the CO adlayer generated by the electroreduction of CO_2, only a single, even broader band, at a frequency characteristic of CO_L is seen in CO-saturated solutions. We

attribute this to the lower coverage of the adlayer formed upon reduction of CO_2, which leads to a lower degree of dipole-dipole coupling. Upon reversing the direction of the sweep in the CV, the intensity of the CO bands continues increasing for as long as a reduction current flows, but starts decreasing at more positive potentials due to CO desorption from the surface.

KEYWORDS. CO_2 electroreduction; ionic liquids; ATR-SEIRAS; Au; CO.

INTRODUCTION

Electrochemical reduction of CO_2 has received much interest as a potential method of producing hydrocarbon fuels and other marketable products. In aqueous media, the reaction typically suffers from high overpotentials, low faradaic efficiencies due to the competing hydrogen evolution reaction (HER, together resulting in a low energy efficiency), and low product selectivity.[1] It should be noted, though, that reversible interconversion between CO_2 and formate with high faradaic and energetic efficiencies has been shown to be possible using electrodes modified with a tungsten-containing formate dehydrogenase enzyme.[2]

The need for high overpotentials is believed to be due to the large thermodynamic overpotential associated with the formation of the unstable CO_2^- radical in the first electron transfer, which is also believed to be the rate-determining step.[3,4] These limitations have prompted research into alternative electrolytes for CO_2 reduction, including Room-temperature Ionic Liquids (RTILs). RTILs have negligible vapour pressures, high electric conductivity, wide electrochemical windows, and high thermal stability. In addition, the high solubility of CO_2 in RTILs makes them particularly attractive for CO_2 capture and conversion. (CO_2 solubility at 1 atm was found to be

around 0.10 mol dm^{-3} for a series of imidazolium-based RTILs,[5] compared with 0.03 mol dm^{-3} in water.)

Rosen et al.[6] recently reported the reduction of CO_2 to CO on Ag electrodes in 1-ethyl-3-methylimidazolium tetrafluoroborate (EMIM-BF_4) / water (18% mol / mol) with high faradaic efficiency and at low overpotentials, resulting in high energy efficiencies. The low overpotential was attributed to a stabilisation of the CO_2^- radical by complexation with the $[EMIM]^+$ cation, hence significantly reducing the thermodynamic overpotential for CO_2 reduction.[7] This hypothesis was challenged in a recent review by Savéant and co-workers,[8] who argue that this complex would be unlikely to have such a strong effect on the energetics of the reaction. Rather, they suggest that the low overpotentials cannot be attributed to the RTIL alone, and the electrode material must play a crucial role in facilitating CO_2 reduction. This was supported by very recent experimental results from Tanner et al., who showed that there is a silver-specific enhancement of CO_2 reduction in RTILs.[9] In another very recent report, Lau et al. have provided experimental evidence that the C4 and C5 protons of the imidazolium ring are key for efficient catalysis.[10] In this case, the authors postulate that the co-catalytic effect of imidazolium derives from hydrogen bonding with adsorbed CO_2^- through the C4 and C5 protons.

All the work reported in the paragraphs above was done using classical electrochemical techniques, based on applying a potential perturbation and measuring the response of the current flowing through the system (or *vice versa*). Although current and potential can be controlled and measured with high precision, classical electrochemical techniques cannot provide direct information on the intermediates formed during electrochemical reactions. The latter can be achieved by coupling a suitable spectroscopic technique to the electrochemical experiment. However, the number of *in-situ* spectroelectrochemical studies of the electroreduction of CO_2 is

still limited.[3,7,11–26] Using Sum Frequency Generation (SFG) to study CO_2 reduction on Pt electrodes in EMIM-BF_4, Braunschweig et al. [16] recently claimed the detection of an $[EMIM]^+$-CO_2 complex with an antisymmetric O–C–O stretching frequency of 2355 cm^{-1}. This blue shift (this band typically appears at 2343 cm^{-1}) interestingly suggests a strengthened C-O bond, as noted by the authors. Their data also show adsorbed CO (CO_{ad}) appearing only after repeated potential cycling, accumulating during positive-going potential sweeps, and disappearing in negative-going potential sweeps, a very surprising behaviour for the product of an electrochemical reduction.

Surface-enhanced infrared absorption spectroscopy in the attenuated total reflection mode (ATR-SEIRAS) has some advantages with respect to SFG or infrared reflection-absorption spectroscopy (IRRAS). Although not interface-selective like SFG, it still has a strong surface sensitivity due to the short range of the SEIRAS effect (ca. 10 nm from the metal surface[27]). In addition, in the ATR geometry the IR beam does not need to cross through the electrolyte, resulting in much less interference from the bulk electrolyte than in IRRAS, and in much smaller electrolyte resistance than in the thin-layer configuration required for both SFG and IRRAS. Finally, the thin-layer configuration characteristic of both SFG and IRRAS also results in seriously impeded transport of electroactive species to the electrode surface, which makes the study of electrocatalytic reactions under continuous supply of reactants (and diffusion of products away from the surface) impossible. Developed in the 1990s by Osawa,[27–33] ATR-SEIRAS has since been successfully applied to the study of the structure of the electrical double layer,[30,34–36] as well as to many electrocatalytic processes.[24,37–42]

Herein, we report the results of the first ATR-SEIRAS investigation of the electroreduction of CO_2 on an Au electrode in an ionic liquid / water mixture. This is preceded by a brief ATR-

SEIRAS study of the changes in the structure of the interface due to double-layer charging in the absence of CO_2, and, since CO is the main, if not the only, product of CO_2 reduction on Au,[1] by a brief ATR-SEIRAS study of CO adsorption on Au in the ionic liquid / water mixture. Additional studies involving Pt and Ag electrodes will be reported in forthcoming contributions.

EXPERIMENTAL SECTION

ATR-SEIRA spectra were recorded using a Nicolet 470 FTIR spectrometer equipped with an MCT detector and a homemade ATR accessory, using unpolarised light. Differential spectra are reported in absorbance units, calculated as $-\log(R_{sample} / R_{reference})$, where $R_{reference}$ and R_{sample} are the reference and sample spectra, respectively. Spectral series were obtained in the spectrometer's kinetics mode by accumulating 95 interferograms with a resolution of 4 cm^{-1} while sweeping the potential at 5 x 10^{-4} V s^{-1}. The time interval between spectra was 20.11 s, corresponding to a potential interval of 10.1 mV. Alternatively, potential-step differential spectra were obtained by accumulating 200 interferograms, also with a resolution of 4 cm^{-1}. The electrode potential was controlled with an EmStat3 mini USB potentiostat (PalmSens).

The ATR infrared spectrum of the [EMIM]BF_4 / H_2O mixture was recorded by covering the surface of a Si prism with a liquid film of the mixture, using the spectrum of the dry Si prism as background. Both the background and sample spectra consisted of 100 interferograms with a spectral resolution of 4 cm^{-1}.

The working electrode was a polycrystalline Au thin-film electrode deposited chemically on a Si prism bevelled at 60 degrees following a previously reported procedure.[43] The Au-covered Si prism was attached to the spectroelectrochemical cell using an O-ring seal. Electrical contact to the film was made by pressing onto it a circular gold wire. Prior to any IR measurements, the

electrode was cycled repetitively in 0.1 M $HClO_4$. The cell was then rinsed thoroughly with Ultrapure water (MilliQ) and air-dried before the [EMIM]BF_4 / H_2O mixture was introduced. The counter electrode was either a graphite rod or an Au wire immersed in the counter-electrode compartment, separated from the main cell compartment by a glass frit. A Pt wire (Alfa Aesar, 99.997% metals basis), flame-annealed before each experiment, was used as a quasi-reference electrode. [EMIM]BF_4 was purchased from Sigma-Aldrich (98% pure), and was used as received. The working electrolyte was prepared by mixing [EMIM]BF_4 with ultrapure water to an 18% molar fraction of [EMIM]BF_4.

RESULTS AND DISCUSSION

Cyclic voltammograms (CVs) recorded at $5x10^{-4}$ V s^{-1} in N_2-purged and CO_2-saturated [EMIM]BF_4 / water mixtures (18 mol % EMIM-BF_4), respectively, are shown in Fig. 1. In the absence of CO_2, hydrogen evolution due to reduction of H_2O reaches a current density of ca. 0.2 mA cm^{-2} at −1.3 V. A much larger current is observed in CO_2-saturated solution, which we attribute to the electroreduction of CO_2.

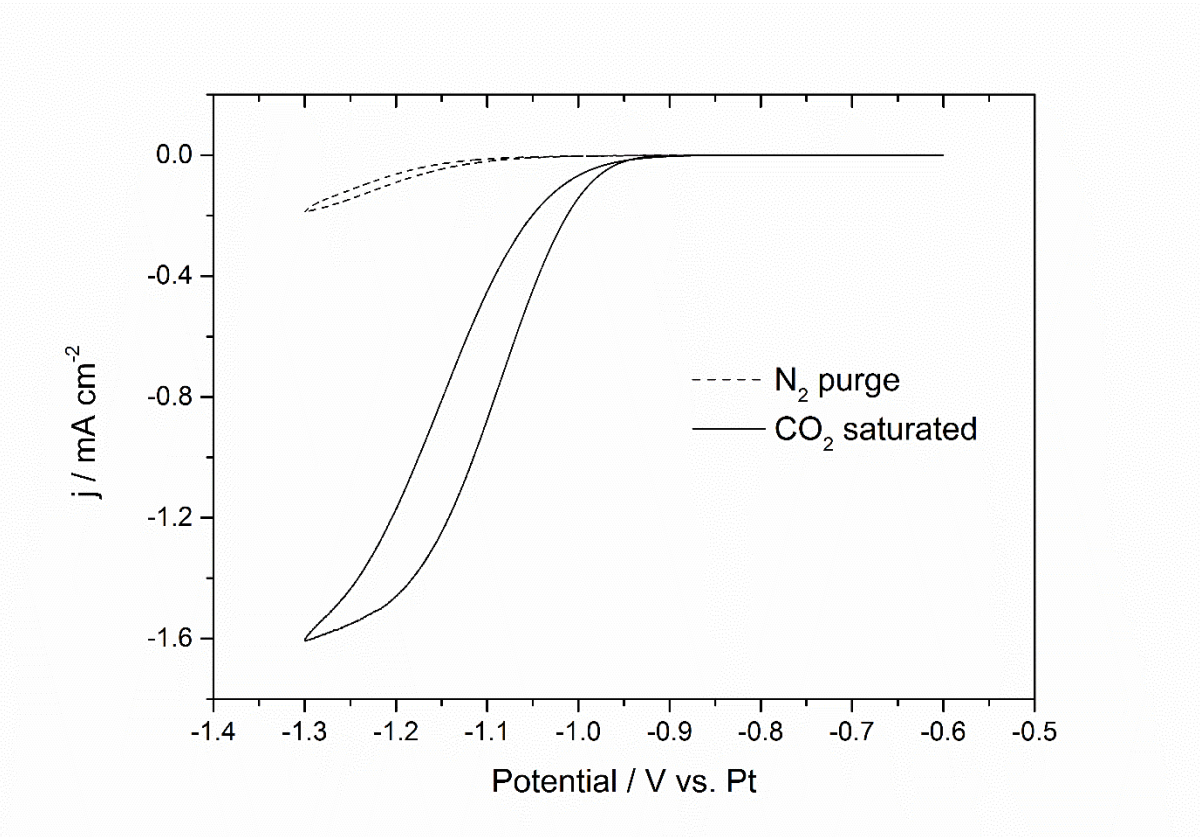

Figure 1. Cyclic voltammograms at $5x10^{-4}$ V s^{-1} of an Au electrode in [EMIM]BF_4 / H_2O mixture (18 mol % EMIM-BF_4) purged with N_2 (dashed line), and saturated with CO_2 (solid line).

1. **Double-layer charging in the absence of CO_2.** The ATR infrared spectrum of the [EMIM]BF_4 / water mixture (18 mol % EMIM-BF_4) is shown in Fig. 2 (red lines). Two bands can be clearly observed in the O–H stretching region (ν(OH)): a sharper peak at 3610 cm^{-1} and a broad peak centred on 3400 cm^{-1}. The former is surprisingly close to the symmetric O–H stretching frequency (ν_{sym}(OH)) of a water monomer (3657 cm^{-1}),[44] suggesting the presence of water with a low degree of hydrogen bonding, whereas the latter is typical of bulk water with a higher degree of hydrogen bonding. We attribute these two peaks to two different populations of water, namely, water in an RTIL-rich environment

(3610 cm^{-1}) and bulk-like water (3400 cm^{-1}). The bands at 3166 and 3125 cm^{-1} correspond to the in-phase stretching of the C(4)–H and C(5)–H bonds, and to the C(2)–H stretching, respectively.[45] The band at 1636 cm^{-1} is assigned to the H–O–H bending mode of H_2O (δ(H–O–H)), while the band at 1576 cm^{-1} has been attributed to the C=C stretching of the $EMIM^+$ ion.[45] Two other weaker bands attributable to $EMIM^+$ can be observed at 1458 and 1358 cm^{-1}, corresponding to the asymmetric CH_3 bending ($\delta_{as}(CH_3)$) of the methyl group and to the wagging mode of the CH_2 group ($w(CH_2)$), respectively.[45] The band at 1171 cm^{-1} corresponds to the stretching of the methyl–N and the ethyl–N bonds.[45] These bands can be better appreciated in Fig. S1.

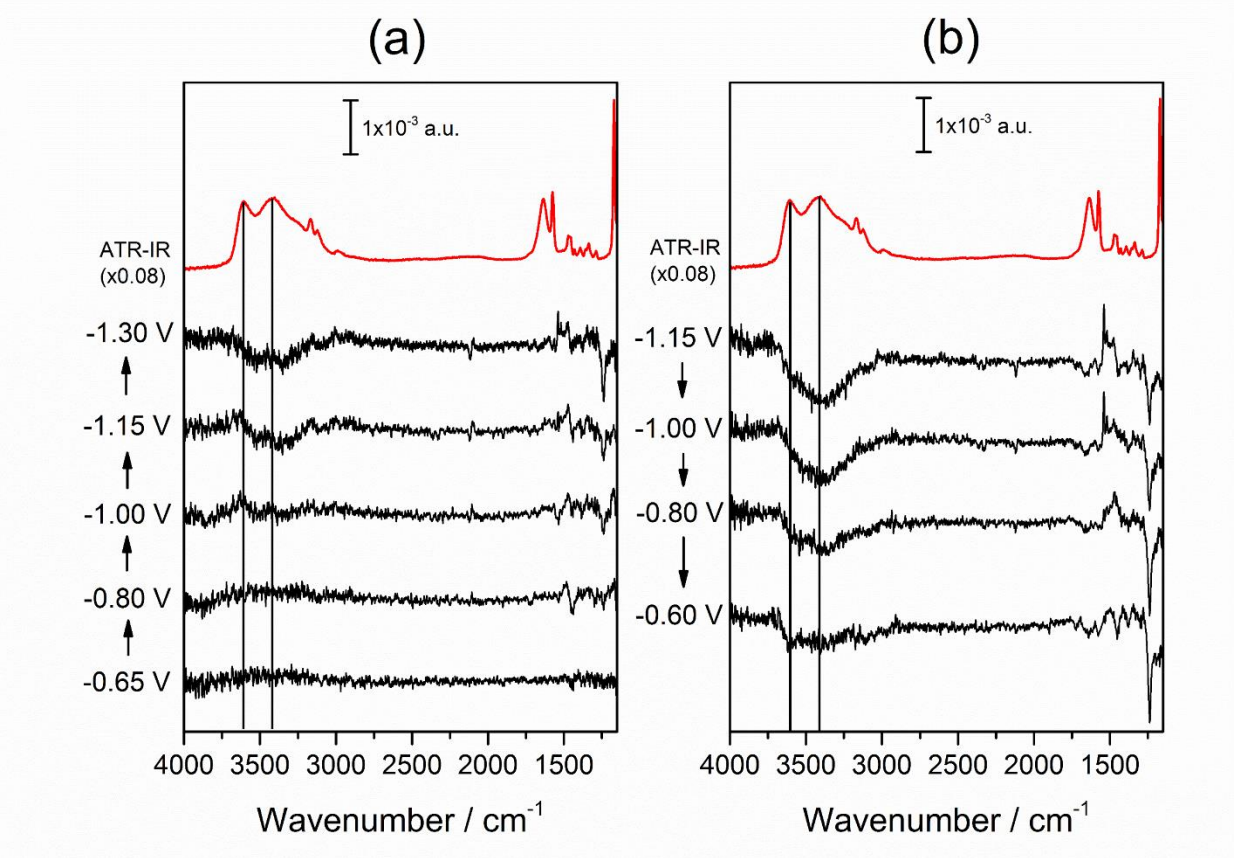

Figure 2. ATR-SEIRA spectra of the Au-electrolyte interface collected at during a cyclic voltammogram between -0.60 and -1.3 V at 5 x 10^{-4} V s^{-1} in N_2-purged [EMIM]BF_4 / H_2O mixture (18% mol / mol), using the spectrum recorded at −0.60 V as reference. For the sake of clarity, the spectral series has been split into two sections, corresponding to the negative-going sweep (a) and the positive-going sweep (b), respectively. The red lines correspond to the ATR infrared spectrum of the [EMIM]BF_4 / H_2O mixture (18% mol / mol), and are included for the sake of comparison.

Figure 2 also shows a selection of ATR-SEIRA spectra collected during a cyclic voltammogram starting at −0.60 V and with a negative potential limit of −1.30 V in N_2-saturated electrolyte (black lines). During the negative-going sweep (Figure 2(a)), two positive bands appear between 1500 and 1550 cm^{-1} which are completely absent in the transmission spectrum of the [EMIM]BF_4 / H_2O mixture (Figure 2, red lines). We attribute these bands to some impurity present in the commercial [EMIM]BF_4 used, which accumulates at the interface at negative potentials. Although the appearance of these bands in Figure 2 appears to be related to the onset of the Faradaic current (see Figure 1), in other experiments we found they appeared in potential regions where only double layer charging current was present. Therefore, we do not believe these bands to be generated due to the decomposition of the ionic liquid. The possibility that the bands arise from a vibrational mode of $EMIM^+$ inactive in IR which becomes active due to symmetry breaking at the electrode-electrolyte interface must also be discarded, because $EMIM^+$ belongs to the C_s symmetry group, and all its vibrations are IR and Raman active. BF_4^- cannot be responsible for these bands either because it has no vibrational modes at frequencies above 1115 cm^{-1}.[46] Unfortunately, we are yet to identify the impurity responsible for these bands. The downward-pointing band centred around 1240 cm^{-1} is due to the Si-O stretching.[13]

Positive bands at 1472 and 1455 cm^{-1} at−1.20 V in Fig. 2(a) indicate that the interface is enriched with $EMIM^{+}$ cations. This effect is better appreciated in the potential-difference ATR-SEIRA spectrum in Fig. S1, obtained after a potential step from -0.6 to -1.20 V. The behaviour of the OH-stretching bands of water is much more complex, with a positive band at 3610 cm-^{1} slightly increasing initially, and both the 3610 and 3400 cm-1 turning negative below -1.15 V. Both bands remain negative during the positive-going sweep until going back to essentially the original background at -0.60 V. Interestingly, the behaviour is different when a potential step is applied from -0.60 to -1.20 V, as illustrated in Fig. S1. In this case, two small positive bands at 3610 and 3415 cm^{-1} can be observed, although their relative intensities have changed as compared to the transmission spectrum. This suggests an increase of the concentration of both types of water (water in an RTIL-rich environment and bulk-like water) at the interface at negative potentials, with the latter increasing more than the former. We have no explanation for this different behaviour of interfacial water when a potential step is applied as opposed to a slow potential sweep, but it suggests some irreversibility of the double-layer charging process, a well-known phenomenon in ionic-liquid based electrolytes.[47–50] Interestingly, and despite the concentration of water in our case being considerably larger than the 700 ppm used by Motobayashi and Osawa, we do not observe any evidence of the interfacial, hydrogen-down, water layer typically found at the Au / water interface at 3507 cm^{-1} at negative potentials.[30]

2. CO adsorption on Au electrodes in [EMIM]BF_4 / water mixtures. Fig. 3 shows the ATR-SEIRA spectrum of an Au electrode in CO-saturated [EMIM]BF_4 / H_2O mixture (18% mol / mol) at −1.30 V . The reference spectrum was collected at −0.60 V in the absence of CO in the electrolyte. Only one band at 1915 cm^{-1}, which we attribute to linearly adsorbed CO (CO_L) on Au, can be observed in the spectrum. This is close to the frequency range between 1940 and 1980 cm-

[1] in which bands for CO_L on Au are typically observed in strongly alkaline solutions saturated with CO,[51] where CO adsorption on Au is stronger than in acidic medium.[52] The lower frequency observed here suggests that, in the absolute potential scale, the potential region covered here may be even more negative than the potential window accessible in strongly alkaline aqueous solutions. Our assignment is confirmed by comparison with spectra of CO_{ad} on a Pt electrode in the same medium (Fig. S2). The frequency of the CO_L band on Pt increases with increasing potential at a rate of ca. 36 cm^{-1} V^{-1}, similar to values reported in aqueous electrolytes.[53,54] At −1.20 V vs. Pt the stretching frequency of CO_L on Pt in [EMIM]BF_4 / H_2O (18% mol / mol) is 2025 cm^{-1}. Extrapolating from the frequencies typically observed in aqueous media[55,56] by using a Stark tuning rate of 30 cm^{-1} V^{-1} we estimate that a band at this frequency would be observed around −1.30 V vs. SHE in aqueous media (in other words, that −1.20 V vs. Pt in [EMIM]BF_4 / H_2O (18% mol / mol) corresponds to −1.30 V vs. SHE in an aqueous electrolyte). This implies that the spectrum in Fig. 2 was recorded at an absolute potential ca. 0.5 V more negative than the most negative potential used by Kunimatsu et al.,[51] accounting for the lower frequency and confirming our assignment of the 1915 cm^{-1} band to CO_L on Au.

The CO_L band in Fig. 3 shows an anomalously large inhomogenous broadening, which results in a large full width at medium height (FWMH) of 150 cm^{-1} (compare with a typical FWMH of ca. 13 cm^{-1} for a saturated CO adlayer on polycrystalline Pt in aqueous electrolytes, or of ca. 28 cm^{-1} for CO_L on Au in acidic aqueous solution[57]), and gives the band an asymmetric aspect, with a clear tailing to lower frequencies. Inhomogeneous broadening of infrared absorption bands is the consequence of dipole-dipole coupling between dipoles oscillating at distinct but similar frequencies. [58,59] In addition to a shift to higher frequencies of the absorption band, dipole-dipole coupling also results in a transfer of intensity from the lower-frequency band to that appearing at

higher frequency. As a consequence, typically only the band at higher frequency is observed (even if it corresponds to the minority species[59]), although with a tail extending to lower frequencies that causes asymmetry. The broad band in Fig. 3 suggests a large multiplicity of sites. We must note, however, that dipole-dipole coupling is small for dipoles whose oscillating frequencies differ by more than 100 cm^{-1}, and usually negligible for differences above 200 cm^{-1}.[59] The apparent strong coupling between dipoles oscillating in the frequency range between ca. 1750 and 2000 cm^{-1}, which we believe is the reason why the band CO_B observed upon reduction of CO_2 (see below) cannot be resolved from the CO_L band in CO-saturated solution, is, therefore, quite remarkable.

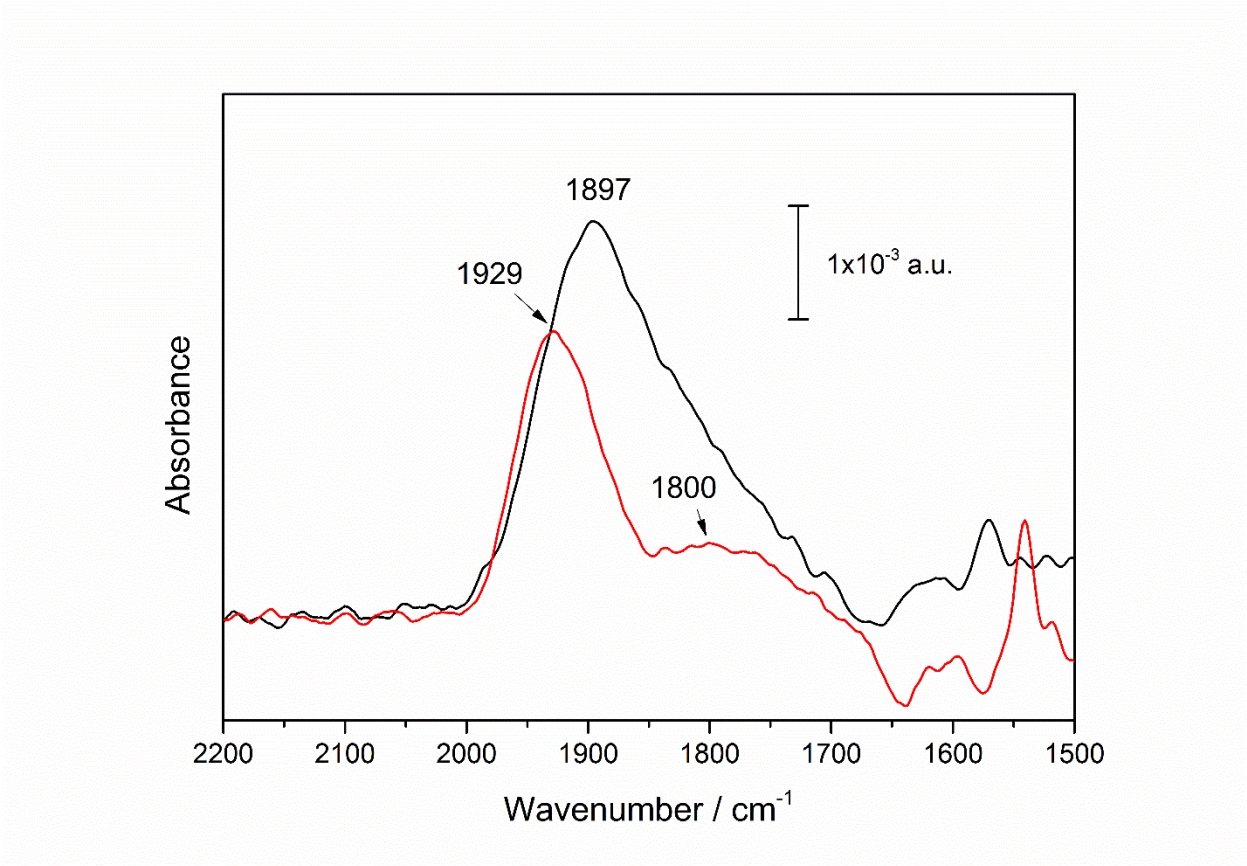

Figure 3. ATR-SEIRA spectra of CO adsorbed on Au at −1.30 V *vs.* Pt in CO-saturated (black line) and in CO_2-saturated [EMIM]BF_4 / H_2O mixture (18% mol / mol). The reference spectra were taken at −0.60 V in the absence of CO and in CO_2-saturated electrolyte, respectively.

3. CO_2 electroreduction on Au in [EMIM]BF_4 / H_2O (18% mol / mol). Potential-dependent ATR-SEIRA spectra, acquired during a CV at 5 x 10^{-4} V s^{-1} in CO_2-saturated [EMIM]BF_4 / H_2O using the spectrum at −0.60 V as reference, are shown in Fig. 4, and Fig. 5 compares the current in the CV with the integrated intensities of the bands corresponding to CO_2 at the interface and CO_L. During the negative-going sweep (Fig. 4a), a negative band at 2343 cm^{-1}, indicating a decrease in the concentration of CO_2 at the interface, becomes apparent just below −1.00 V, when the reduction current is ca. 0.2 mA cm^{-2}. The delay in the appearance of this band with respect to the onset of the reduction current (ca. −0.95 V) may indicate that in the potential range between −0.95 V and −1.10 V the rate of the reaction is slower than the diffusion of CO_2 from the bulk to the interface, where the change in its concentration is below the detection limit. A positive band around 1910 cm^{-1}, attributed to CO_L on Au, generated by the electroreduction of CO_2, becomes apparent at −1.20 V. Both the positive CO_L and the negative CO_2 bands continue to grow (albeit in opposite directions) until −1.30 V (see Fig. 4a and Fig. 5b and c). An upward pointing shoulder at ca. 1750 cm^{-1} appears at −1.25 V and grows together with the CO_L band as the potential is made more negative. We assign this band to bridge-bonded adsorbed CO on Au (CO_B). CO_L and CO_B have also been detected on Au as intermediates in the of reduction of CO_2 to CO(g) in aqueous electrolyte.[25]

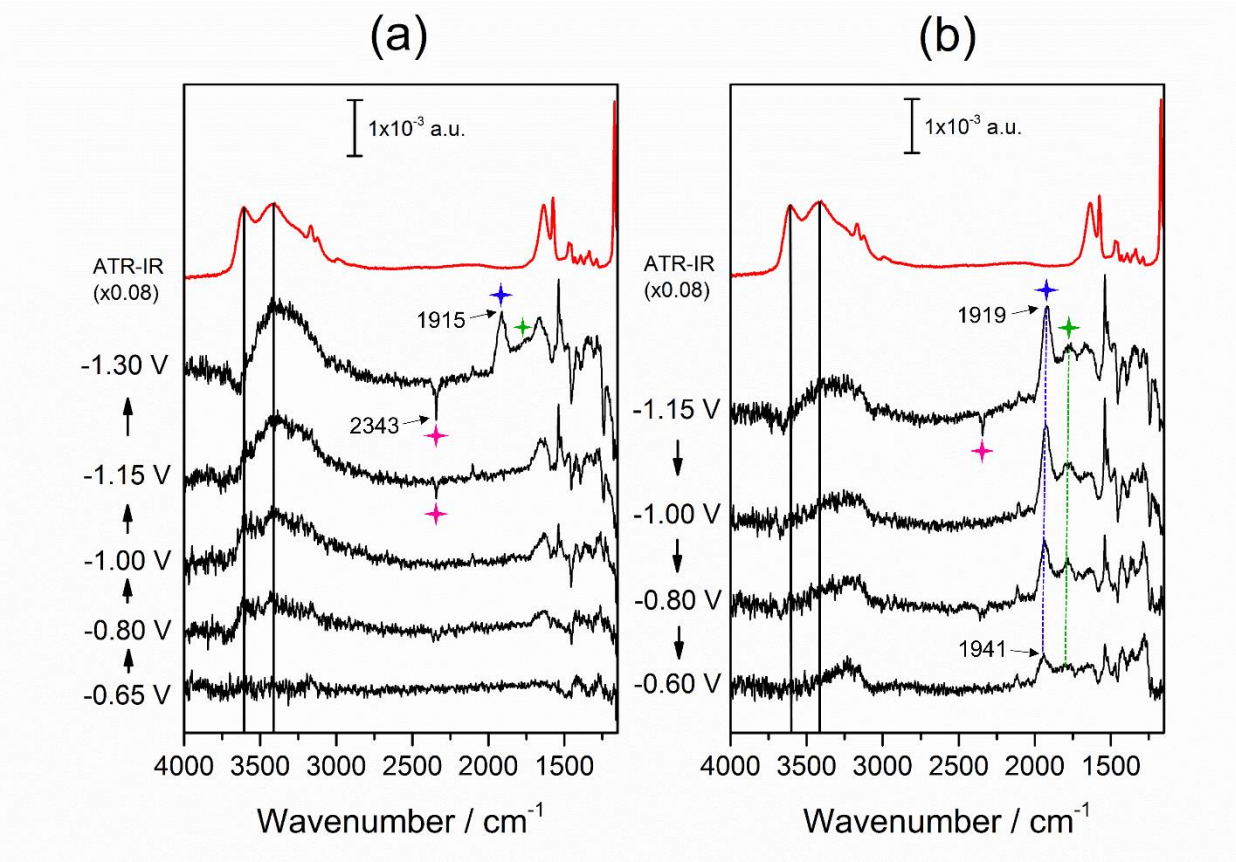

Figure 4. ATR-SEIRA spectra of an Au electrode in CO_2-saturated [EMIM]BF_4 / water (18% mol / mol) acquired during the negative-going (a) and positive-going (b) sweeps of a cyclic voltammogram at $5x10^{-4}$ V s^{-1}. The reference spectrum was taken at −0.60 V just before starting the potential sweep in the negative direction. The highlighted bands correspond to $\nu_{asym}(CO_2)$ ✦ ; $\nu(CO_L)$ ✦ and $\nu(CO_B)$ ✦. The red lines correspond to the ATR infrared spectrum of the [EMIM]BF_4 / H_2O mixture (18% mol / mol), and are included for the sake of comparison.

In a separate experiment, the potential was stepped from −0.60 V (where, according to the CV, no CO_2 reduction takes place) to −1.30 V, and the evolution of the ATR-SEIRA spectrum was recorded for 23 minutes (Fig. S3). A band at 1912 cm^{-1}corresponding to CO_L emerges immediately, an additional band at 1785 cm^{-1} corresponding to CO_B emerging after 7 minutes at −1.30 V. Both signals show an increase in intensity and a blue shift with increasing time. This

confirms that both bands emerge as a consequence of CO_2 reduction, and that they belong to adsorbed species.

The infrared spectrum of CO_{ad} generated upon reduction of CO_2 is different to that corresponding to CO_{ad} from a CO-saturated solution, as illustrated in Fig.3 (red and black lines, respectively). Interestingly, the CO_B band is not observed in the latter case, in which the CO_L band is also anomalously broad and very asymmetric, as we have discussed above. The absence of the CO_B band in CO-saturated electrolyte might be due to a higher overall θ_{CO}, which would favour intensity stealing by dipoles oscillating at higher frequency via dipole-dipole coupling. This phenomenon might be absent in the CO adlayers generated upon CO_2 reduction due to a lower θ_{CO}, which would allow the CO_B band to appear decoupled from CO_L. It might also suggest that CO_{ad} generated from the electroreduction of CO_2 has a lower multiplicity of sites, leading to a decoupling of the CO_L and CO_B bands, in contrast with experiments in CO-saturated electrolyte (Fig. 3). In this regard, it is also worth noting that, despite the expectedly lower coverage, the CO_L band resulting from CO_2 reduction appears at a slightly higher frequency than that resulting from direct adsorption of CO (1929 vs. 1915 cm^{-1}), and that the former also exhibits a smaller FWMH than the latter (73 vs. 150 cm^{-1}). In those cases in which CO adsorbs weakly on the metal surface, like Au, Ag or Cu, the C–O stretching band is expected to appear at higher frequencies for CO_{ad} on step sites.[44] Although we cannot offer a definite explanation for these observations, we believe that they might be related with CO_2 being formed faster at step sites (it has been shown that a higher density of grain boundaries in Au nanoparticles results in a higher catalytic activity for CO_2 reduction[60]), leading to a higher steady-state coverage of CO_{ad} on steps compared to CO_{ad} on terraces, and to a lower multiplicity of adsorption sites. The FWHM of the band of CO_L generated upon CO_2 reduction in our [EMIM]BF_4 / H_2O mixture is

also larger than that of the same species formed by reduction of CO_2 in aqueous HCO_3^-/CO_2 buffers.[25]

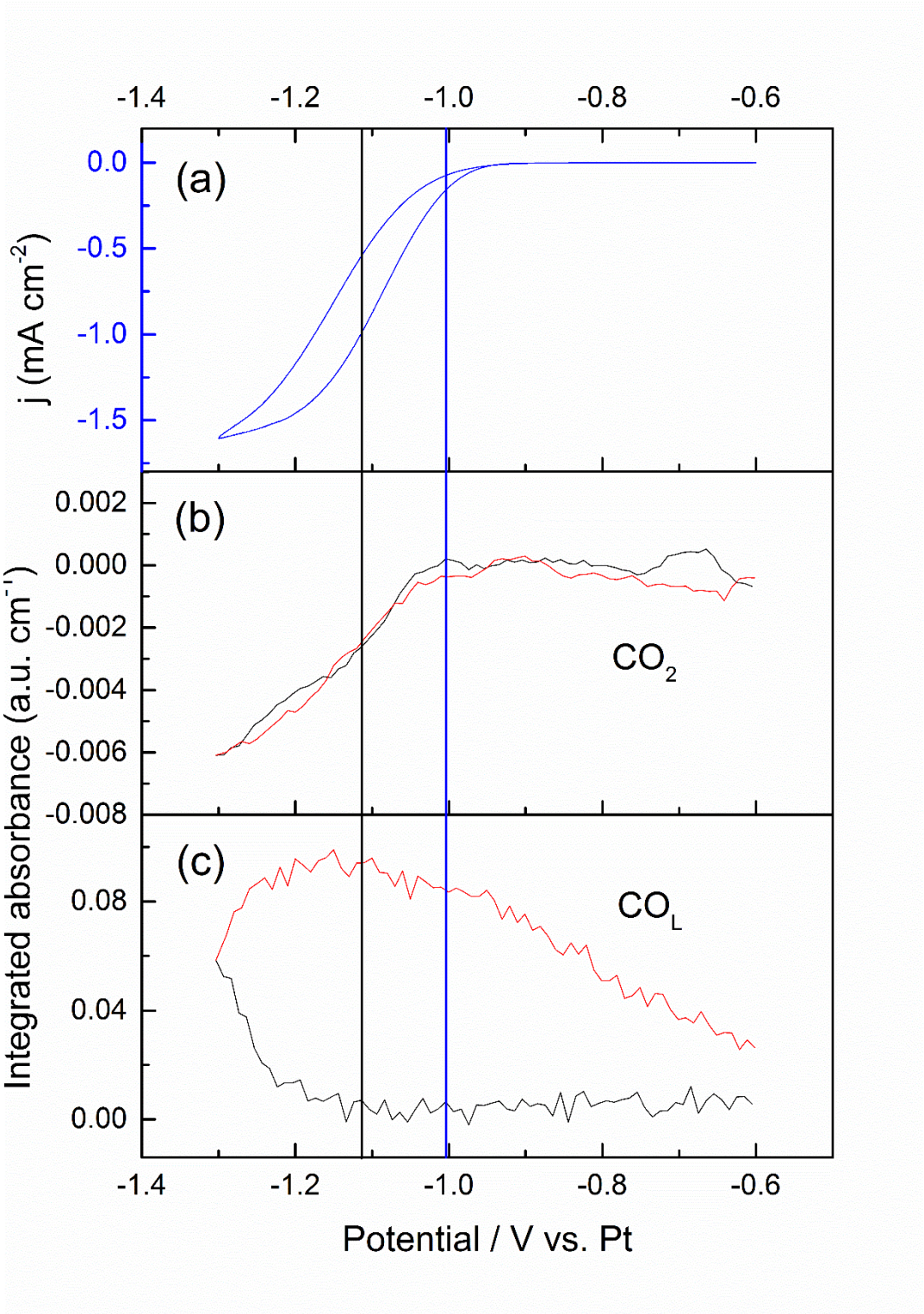

Figure 5. Potential dependence of the integrated absorption of the CO_L (b) and CO_2 (c) bands obtained from a series of ATR-SEIRA spectra recorded simultaneously with the CV (5×10^{-4} V s^{-1}) shown in (a). The black and red traces in (b) and (c) are for the negative- and positive-going potential sweep, respectively. The blue and black vertical lines show the potential at which the negative-absorbance CO_2 band and the positive-absorbance CO_L band, respectively, emerge.

As illustrated in Fig. 5, the CO_L (and the CO_B, not shown) band continues increasing in intensity after reversing the direction of the potential sweep at −1.30 V, until approximately −1.10 V, suggesting that θ_{CO} continues increasing in this potential region during the positive potential sweep. This was to be expected, as the current in the CV (Fig. 1 and Fig. 5a) remains negative (i.e., CO_2 keeps being reduced) up to approximately −0.95 V. Both bands shift to higher frequencies during the positive-going sweep (Fig. 4b), which must result from a combination of an increase in dipole-dipole coupling due to the increase in θ_{CO} between -1.30 and -1.15 V (see Fig. 5), and the Stark shift.

The behaviour of the CO_{ad} bands reported in Figs. 4 and 5 is that expected for the product of a reduction, and is the opposite of that recently reported for CO_{ad} formed during the electroreduction of CO_2 on Pt in dry [EMIM]BF_4.[16] Experiments similar to those reported here but using a Pt electrode, which will be reported in due course, yield similar results, excluding the possibility that the difference between the behaviour reported here and that reported previously[16] is due to the use of a different substrate. Also in contradiction with that report, both in the case of Au and Pt electrodes CO_{ad} is observed already in the first negative sweep, and no need for repeated potential cycling was found.

Negative $EMIM^+$ bands at 1455 and 1575 cm^{-1} were observed in the negative-going sweep in CO_2-saturated solution (Fig. 4a), in contrast with the positive bands at the same frequency observed in the absence of CO_2 (Fig. 2). These negative absorption bands become more intense with increasing negative potential, suggesting that the reorientation of $EMIM^+$ upon double layer charging is different when CO_2 is present. This could be due to the presence of CO_{ad} generated upon CO_2 reduction, as the charge density on the electrode surface when covered by CO_{ad} can be expected to be different to that of the naked surface.[61]

The bands in the O-H stretching region are also different in CO_2-free (Fig. 2) and in CO_2-containing (Figure 4) electrolytes. In the latter case, a broad positive band at 3500-3100 cm^{-1} and a positive band centred around 1636 cm^{-1}, corresponding respectively to ν(OH) and δ(H–O–H) of bulk-like water, appear during the negative-going sweep. Their intensity increases until −1.20 V, and then remains constant until −1.30 V. Interestingly, and contrary to what happens in the absence of CO_2, at −1.25 V a sharper negative band emerges at 3610 cm^{-1}, which we have assigned above to ν(OH) of water in an RTIL-rich environment. This might be related to the different rearrangement of the cations as the CO_{ad}-covered surface is charged negatively, as discussed above, or might also indicate a preference for water in an RTIL-rich environment as the proton donor in the electroreduction of CO_2 to CO.

As shown in Fig. 5, the intensity of the negative CO_2 band grows in parallel with the current, which is a good indication that the latter is due to the electroreduction of CO_2. On the other hand, the CO_L band emerges at −1.20 V. Taking into account that CO adsorbs relatively weakly on Au, the appearance of the CO_L band at −1.20 V may be explained by the necessity to build up a sufficiently high concentration of CO at the interface before a detectable θ_{CO} is reached. This

hypothesis is supported by the observation that the intensity of the CO_L band starts decreasing steadily after reaching a maximum at −1.15 V in the reverse, positive-going sweep. As no oxidation current can be observed in the simultaneously recorded CV (Fig. 5), the decrease in θ_{CO} can only be attributed to the desorption of CO from the surface (which, after all, must be the last step in the reduction of CO_2(g) to CO(g)). The final spectrum, taken at −0.60 V, shows that a small amount of both CO_L and CO_B remain adsorbed on the Au electrode.

CONCLUDING REMARKS

Combining *in-situ* ATR-SEIRAS with cyclic voltammetry, we have shown that the negative current observed on an Au electrode in CO_2-saturated [EMIM]BF_4 / water 18% (mol / mol) at potentials more negative than ca. −1.0 V vs. Pt corresponds to the electroreduction of CO_2. Electroreduction of CO_2 results in the formation of CO_{ad}, whose coverage increases with increasing negative potential, and appears to establish an equilibrium with dissolved CO in the electrolyte. Infrared spectroscopy reveals the presence of two types of water in the [EMIM]BF_4 / water mixture, with different degrees of hydrogen bonding, which we have attributed to water in water-rich regions (bulk-like water) and water in an RTIL-rich environment. Interestingly, in the presence of CO_2 only bulk-like water accumulates at the interface at negative potentials, while water associated to an RTIL-rich environment is depleted from it. This could indicate the preferential use of this kind of water as a proton donor for the reduction of CO_2. Both CO_L and CO_B are detected as a product of the reduction of CO_2, although only CO_L was detected when adsorption occurred from a CO-saturated solution. This discrepancy was attributed to a lower θ_{CO} when CO_{ad} is formed from the reduction of CO_2, preventing dipole-dipole coupling between the two CO_{ad} species. No spectroscopic evidence of reduction intermediates or $EMIM^+$-CO_2 complexes could be found.

Our work emphasizes the importance of applying highly sensitive spectroscopic techniques to study complex electrocatalytic reactions in complex electrolytic media. This strategy yielded in the last decades an exponential increase of our understanding of electrochemical processes in comparatively simple aqueous electrolyte, but has not been intensively applied to RTILs and other complex systems yet. The application of ATR-SEIRAS and other techniques that can provide information regarding the composition of the interface in real time, instead of exclusively relying in purely electrochemical experiments and techniques that can only analyse the product composition after prolonged electrolysis, is necessary for a deeper understanding of systems with a high degree of complexity, like the electroreduction of CO_2 in RTILs.

ASSOCIATED CONTENT

Supporting Information. The following files are available free of charge.

Figures S1 to S3 (PDF)

AUTHOR INFORMATION

Corresponding Author

*angel.cuestaciscar@abdn.ac.uk.

ACKNOWLEDGMENTS

The support of the University of Aberdeen and the Leverhulme Trust (Grant RPG-2015-040) is gratefully acknowledged.

REFERENCES

(1) Hori, Y. Electrochemical CO_2 Reduction on Metal Electrodes. In *Modern Aspects of Electrochemistry*; Vayenas, C. G., White, R. E., Gamboa-Aldeco, M. E., Eds.; Springer:

New York, 2008; Vol. 42, pp 89–189.

(2) Reda, T.; Plugge, C. M.; Abram, N. J.; Hirst, J. Reversible Interconversion of Carbon Dioxide and Formate by an Electroactive Enzyme. *Proc. Natl. Acad. Sci.* **2008**, *105*, 10654–10658.

(3) Chandrasekaran, K.; Bockris, J. O. In-Situ Spectroscopic Investigation of Adsorbed Intermediate Radicals in Electrochemical Reactions: CO_2^- on Platinum. *Surf. Sci.* **1987**, *185*, 495–514.

(4) Bockris, J. O.; Wass, J. C. The Photoelectrocatalytic Reduction of Carbon Dioxide. *J. Electrochem. Soc.* **1989**, *136*, 2521.

(5) Moganty, S. S.; Baltus, R. E. Regular Solution Theory for Low Pressure Carbon Dioxide Solubility in Room Temperature Ionic Liquids: Ionic Liquid Solubility Parameter from Activation Energy of Viscosity. *Ind. Eng. Chem. Res.* **2010**, *49*, 5846–5853.

(6) Rosen, B. A.; Salehi-Khojin, A.; Thorson, M. R.; Zhu, W.; Whipple, D. T.; Kenis, P. J. A.; Masel, R. I. Ionic Liquid–Mediated Selective Conversion of CO_2 to CO at Low Overpotentials. *Science* **2011**, *334*, 643–644.

(7) Rosen, B. A.; Haan, J. L.; Mukherjee, P.; Braunschweig, B.; Zhu, W.; Salehi-Khojin, A.; Dlott, D. D.; Masel, R. I. In Situ Spectroscopic Examination of a Low Overpotential Pathway for Carbon Dioxide Conversion to Carbon Monoxide. *J. Phys. Chem. C* **2012**, *116*, 15307–15312.

(8) Costentin, C.; Robert, M.; Savéant, J.-M. Catalysis of the Electrochemical Reduction of

Carbon Dioxide. *Chem. Soc. Rev.* **2013**, *42*, 2423–2436.

(9) Tanner, E. E. L.; Batchelor-McAuley, C.; Compton, R. G. Carbon Dioxide Reduction in Room-Temperature Ionic Liquids: The Effect of the Choice of Electrode Material, Cation, and Anion. *J. Phys. Chem. C* **2016**, *120*, 26442–26447.

(10) Lau, G. P. S.; Schreier, M.; Vasilyev, D.; Scopelliti, R.; Grätzel, M.; Dyson, P. J. New Insights Into the Role of Imidazolium-Based Promoters for the Electroreduction of CO_2 on a Silver Electrode. *J. Am. Chem. Soc.* **2016**, *138*, 7820–7823.

(11) Dunwell, M.; Xu, B. CO_2 Reduction on Cu at Low Overpotentials with Surface-Enhanced in Situ Spectroscopy. *J. Phys. Chem. C* **2016**, *120*, 17334–17341.

(12) Dunwell, M.; Lu, Q.; Heyes, J. M.; Rosen, J.; Chen, J. G.; Yan, Y.; Jiao, F.; Xu, B. The Central Role of Bicarbonate in the Electrochemical Reduction of Carbon Dioxide on Gold. *J. Am. Chem. Soc.* **2017**, *139*, 3774–3783.

(13) Jiang, K.; Wang, H.; Cai, W.; Wang, H. Li Electrochemical Tuning of Metal Oxide for Highly Selective CO_2 Reduction. *ACS Nano* **2017**, *11*, 6451–6458.

(14) Wang, L.; Gupta, K.; Goodall, J. B. M.; Darr, J. A.; Holt, K. B. In Situ Spectroscopic Monitoring of CO_2 Reduction at Copper Oxide Electrode. *Faraday Discuss.* **2017**, *197*, 517–532.

(15) Ooka, H.; Figueiredo, M. C.; Koper, M. T. M. Competition between Hydrogen Evolution and Carbon Dioxide Reduction on Copper Electrodes in Mildly Acidic Media. *Langmuir* **2017**, *33*, 9307–9313.

(16) Braunschweig, B.; Mukherjee, P.; Haan, J. L.; Dlott, D. D. Vibrational Sum-Frequency Generation Study of the CO_2 Electrochemical Reduction at Pt/EMIM-BF_4 Solid/Liquid Interfaces. *J. Electroanal. Chem.* **2017**, *800*, 144–150.

(17) Gunathunge, C. M.; Li, X.; Li, J.; Hicks, R. P.; Ovalle, V. J.; Waegele, M. M. Spectroscopic Observation of Reversible Surface Reconstruction of Copper Electrodes under CO_2 Reduction. *J. Phys. Chem. C* **2017**, *121*, 12337–12344.

(18) Zhu, S.; Jiang, B.; Cai, W.-B.; Shao, M. Direct Observation on Reaction Intermediates and the Role of Bicarbonate Anions in CO_2 Electrochemical Reduction Reaction on Cu Surfaces. *J. Am. Chem. Soc.* **2017**, *139*, 15664–15667.

(19) Beden, B.; Bewick, A.; Razaq, M.; Weber, J. On the Nature of Reduced CO_2: An IR Spectroscopic Investigation. *J. Electroanal. Chem.* **1982**, *139*, 203–206.

(20) Tomita, Y.; Teruya, S.; Koga, O.; Hori, Y. Electrochemical Reduction of Carbon Dioxide at a Platinum Electrode in Acetonitrile-Water Mixtures. *J. Electrochem. Soc.* **2000**, *147*, 4164.

(21) Smolinka, T.; Heinen, M.; Chen, Y. X.; Jusys, Z.; Lehnert, W.; Behm, R. J. CO_2 Reduction on Pt Electrocatalysts and Its Impact on H_2 Oxidation in CO_2 Containing Fuel Cell Feed Gas - A Combined in Situ Infrared Spectroscopy, Mass Spectrometry and Fuel Cell Performance Study. *Electrochim. Acta* **2005**, *50*, 5189–5199.

(22) García Rey, N.; Dlott, D. D. Structural Transition in an Ionic Liquid Controls CO_2 Electrochemical Reduction. *J. Phys. Chem. C* **2015**, *119*, 20892–20899.

(23) Figueiredo, M. C.; Ledezma-Yanez, I.; Koper, M. T. M. In Situ Spectroscopic Study of CO_2 Electroreduction at Copper Electrodes in Acetonitrile. *ACS Catal.* **2016**, *6*, 2382–2392.

(24) Wuttig, A.; Liu, C.; Peng, Q.; Yaguchi, M.; Hendon, C. H.; Motobayashi, K.; Ye, S.; Osawa, M.; Surendranath, Y. Tracking a Common Surface-Bound Intermediate during CO_2-to-Fuels Catalysis. *ACS Cent. Sci.* **2016**, *2*, 522–528.

(25) Wuttig, A.; Yaguchi, M.; Motobayashi, K.; Osawa, M.; Surendranath, Y. Inhibited Proton Transfer Enhances Au-Catalyzed CO_2-to-Fuels Selectivity. *Proc. Natl. Acad. Sci.* **2016**, *113*, E4585–E4593.

(26) Santos, V. O.; Leite, I. R.; Brolo, A. G.; Rubim, J. C. The Electrochemical Reduction of CO_2 on a Copper Electrode in 1-n-Butyl-3-Methyl Imidazolium Tetrafluoroborate (BMI.BF_4) Monitored by Surface-Enhanced Raman Scattering (SERS). *J. Raman Spectrosc.* **2016**, *47*, 674–680.

(27) Osawa, M.; Ikeda, M. Surface-Enhanced Infrared Absorption of p-Nitrobenzoic Acid Deposited on Silver Island Films: Contributions of Electromagnetic and Chemical Mechanisms. *J. Phys. Chem.* **1991**, *95*, 9914–9919.

(28) Osawa, M.; Ataka, K.; Yoshii, K.; Yotsuyanagi, T. Surface-Enhanced Infrared ATR Spectroscopy for in Situ Studies of Electrode/Electrolyte Interfaces. *J. Electron Spectros. Relat. Phenomena* **1993**, *64–65*, 371–379.

(29) Osawa, M.; Ataka, K.; Yotsuyanagi, T. Real-Time Monitoring of Electrochemical Dynamics by Submillisecond Time-Resolved Surface-Enhanced Infrared Attenuated-Total-Reflection Spectroscopy. *Langmuir* **1994**, *10*, 640–642.

(30) Ataka, K.; Yotsuyanagi, T.; Osawa, M. Potential-Dependent Reorientation of Water Molecules at an Electrode/Electrolyte Interface Studied by Surface-Enhanced Infrared Absorption Spectroscopy. *J. Phys. Chem.* **1996**, *100*, 10664–10672.

(31) Osawa, M. Dynamic Processes in Electrochemical Reactions Studied by Surface-Enhanced Infrared Absorption Spectroscopy (SEIRAS). *Bull. Chem. Soc. Jpn.* **1997**, *70*, 2861–2880.

(32) Osawa, M.; Yoshii, K. In Situ and Real-Time Surface-Enhanced Infrared Study of Electrochemical Reactions. *Appl. Spectrosc.* **1997**, *51*, 512–518.

(33) Osawa, M. Surface-Enhanced Infrared Absorption. In *Near-Field Optics and Surface Plasmon Polaritons*; Kawata, S., Ed.; Springer Berlin Heidelberg: Berlin, Heidelberg, 2001; pp 163–187.

(34) Motobayashi, K.; Osawa, M. Potential-Dependent Condensation of Water at the Interface between Ionic Liquid [BMIM][TFSA] and an Au Electrode. *Electrochem. Commun.* **2016**, *65*, 14–17.

(35) Yamakata, A.; Osawa, M. Destruction of the Water Layer on a Hydrophobic Surface Induced by the Forced Approach of Hydrophilic and Hydrophobic Cations. *J. Phys. Chem. Lett.* **2010**, *1*, 1487–1491.

(36) Yang, Y.-Y.; Zhang, L.-N.; Osawa, M.; Cai, W.-B. Surface-Enhanced Infrared Spectroscopic Study of a CO-Covered Pt Electrode in Room-Temperature Ionic Liquid. *J. Phys. Chem. Lett.* **2013**, *4*, 1582–1586.

(37) Cuesta, A.; Cabello, G.; Gutierrez, C.; Osawa, M. Adsorbed Formate: The Key Intermediate

in the Oxidation of Formic Acid on Platinum Electrodes. *Phys. Chem. Chem. Phys.* **2011**, *13*, 20091–20095.

(38) Cuesta, A.; Cabello, G.; Hartl, F. W.; Escudero-Escribano, M.; Vaz-Domínguez, C.; Kibler, L. A.; Osawa, M.; Gutiérrez, C. Electrooxidation of Formic Acid on Gold: An ATR-SEIRAS Study of the Role of Adsorbed Formate. *Catal. Today* **2013**, *202*, 79–86.

(39) Cuesta, A.; Cabello, G.; Osawa, M.; Gutiérrez, C. Mechanism of the Electrocatalytic Oxidation of Formic Acid on Metals. *ACS Catal.* **2012**, *2*, 728–738.

(40) Chen, Y. X.; Miki, A.; Ye, S.; Sakai, H.; Osawa, M. Formate, an Active Intermediate for Direct Oxidation of Methanol on Pt Electrode. *J. Am. Chem. Soc.* **2003**, *125*, 3680–3681.

(41) Uchida, T.; Mogami, H.; Yamakata, A.; Sasaki, Y.; Osawa, M. Hydrogen Evolution Reaction Catalyzed by Proton-Coupled Redox Cycle of 4,4′-Bipyridine Monolayer Adsorbed on Silver Electrodes. *J. Am. Chem. Soc.* **2008**, *130*, 10862–10863.

(42) Ayemoba, O.; Cuesta, A. Spectroscopic Evidence of Size-Dependent Buffering of Interfacial pH by Cation Hydrolysis during CO_2 Electroreduction. *ACS Appl. Mater. Interfaces* **2017**, *9*, 27377–27382.

(43) Miyake, H.; Ye, S.; Osawa, M. Electroless Deposition of Gold Thin Films on Silicon for Surface-Enhanced Infrared Spectroelectrochemistry. *Electrochem. Commun.* **2002**, *4*, 973–977.

(44) Thiel, P. A.; Madey, T. E. The Interaction of Water with Solid Surfaces: Fundamental Aspects. *Surf. Sci. Rep.* **1987**, *7*, 211–385.

(45) Katsyuba, S. A.; Dyson, P. J.; Vandyukova, E. E.; Chernova, A. V.; Vidis, A. Molecular Structure, Vibrational Spectra, and Hydrogen Bonding of the Ionic Liquid 1-Ethyl-3-Methyl-1H-Imidazolium Tetrafluoroborate. *Helv. Chim. Acta* **2004**, *87*, 2556–2565.

(46) Bates, J. B.; Quist, A. S.; Boyd, G. E. Infrared and Raman Spectra of Polycrystalline $NaBF_4$. *J. Chem. Phys.* **1971**, *54*, 124–126.

(47) Sebastián, P.; Climent, V.; Feliu, J. M. Characterization of the Interfaces between Au(Hkl) Single Crystal Basal Plane Electrodes and [Emmim][Tf_2N] Ionic Liquid. *Electrochem. Commun.* **2016**, *62*, 44–47.

(48) Sebastián, P.; Sandoval, A. P.; Climent, V.; Feliu, J. M. Study of the Interface Pt(111)/ [Emmim][NTf_2] Using Laser-Induced Temperature Jump Experiments. *Electrochem. Commun.* **2015**, *55*, 39–42.

(49) Motobayashi, K.; Minami, K.; Nishi, N.; Sakka, T.; Osawa, M. Hysteresis of Potential-Dependent Changes in Ion Density and Structure of an Ionic Liquid on a Gold Electrode: In Situ Observation by Surface-Enhanced Infrared Absorption Spectroscopy. *J. Phys. Chem. Lett.* **2013**, *4*, 3110–3114.

(50) Uysal, A.; Zhou, H.; Feng, G.; Lee, S. S.; Li, S.; Fenter, P.; Cummings, P. T.; Fulvio, P. F.; Dai, S.; McDonough, J. K.; Gogotsi, Y. Structural Origins of Potential Dependent Hysteresis at the Electrified Graphene/Ionic Liquid Interface. *J. Phys. Chem. C* **2014**, *118*, 569–574.

(51) Kunimatsu, K.; Aramata, A.; Nakajima, N.; Kita, H. Infrared Spectra of Carbon Monoxide Adsorbed on a Smooth Gold Electrode. *J. Electroanal. Chem.* **1986**, *207*, 293–307.

(52) Cuesta, A.; López, N.; Gutiérrez, C. Electrolyte Electroreflectance Study of Carbon Monoxide Adsorption on Polycrystalline Silver and Gold Electrodes. *Electrochim. Acta* **2003**, *48*, 2949–2956.

(53) Kunimatsu, K.; Golden, W. G.; Seki, H.; Philpott, M. R. Carbon Monoxide Adsorption on a Platinum Electrode Studied by Polarization Modulated FT-IRRAS. 1. CO Adsorbed in the Double-Layer Potential Region and Its Oxidation in Acids. *Langmuir* **1985**, *1*, 245–250.

(54) Kunimatsu, K.; Seki, H.; Golden, W. G.; Gordon, J. G.; Philpott, M. R. Carbon Monoxide Adsorption on a Platinum Electrode Studied by Polarization-Modulated FT-IR Reflection-Absorption Spectroscopy: II. Carbon Monoxide Adsorbed at a Potential in the Hydrogen Region and Its Oxidation in Acids. *Langmuir* **1986**, *2*, 464–468.

(55) Cuesta, A.; Couto, A.; Rincón, A.; Pérez, M. C.; López-Cudero, A.; Gutiérrez, C. Potential Dependence of the Saturation CO Coverage of Pt Electrodes: The Origin of the Pre-Peak in CO-Stripping Voltammograms. Part 3: Pt(Poly). *J. Electroanal. Chem.* **2006**, *586*, 184–195.

(56) Silva, C. D.; Cabello, G.; Christinelli, W. A.; Pereira, E. C.; Cuesta, A. Simultaneous Time-Resolved ATR-SEIRAS and CO-Charge Displacement Experiments: The Dynamics of CO Adsorption on Polycrystalline Pt. *J. Electroanal. Chem.* **2017**, *800*, 25–31.

(57) Sun, S.-G.; Cai, W.-B.; Wan, L.-J.; Osawa, M. Infrared Absorption Enhancement for CO Adsorbed on Au Films in Perchloric Acid Solutions and Effects of Surface Structure Studied by Cyclic Voltammetry, Scanning Tunneling Microscopy, and Surface-Enhanced IR Spectroscopy. *J. Phys. Chem. B* **1999**, *103*, 2460–2466.

(58) Hollins, P.; Pritchard, J. Infrared Studies of Chemisorbed Layers on Single Crystals. *Prog.*

Surf. Sci. **1985**, *19*, 275–349.

(59) Hollins, P. The Influence of Surface Defects on the Infrared Spectra of Adsorbed Species. *Surf. Sci. Rep.* **1992**, *16*, 51–94.

(60) Feng, X.; Jiang, K.; Fan, S.; Kanan, M. W. Grain-Boundary-Dependent CO_2 Electroreduction Activity. *J. Am. Chem. Soc.* **2015**, *137*, 4606–4609.

(61) Cuesta, A. Measurement of the Surface Charge Density of CO-Saturated Pt(111) Electrodes as a Function of Potential: The Potential of Zero Charge of Pt(111). *Surf. Sci.* **2004**, *572*, 11–22.

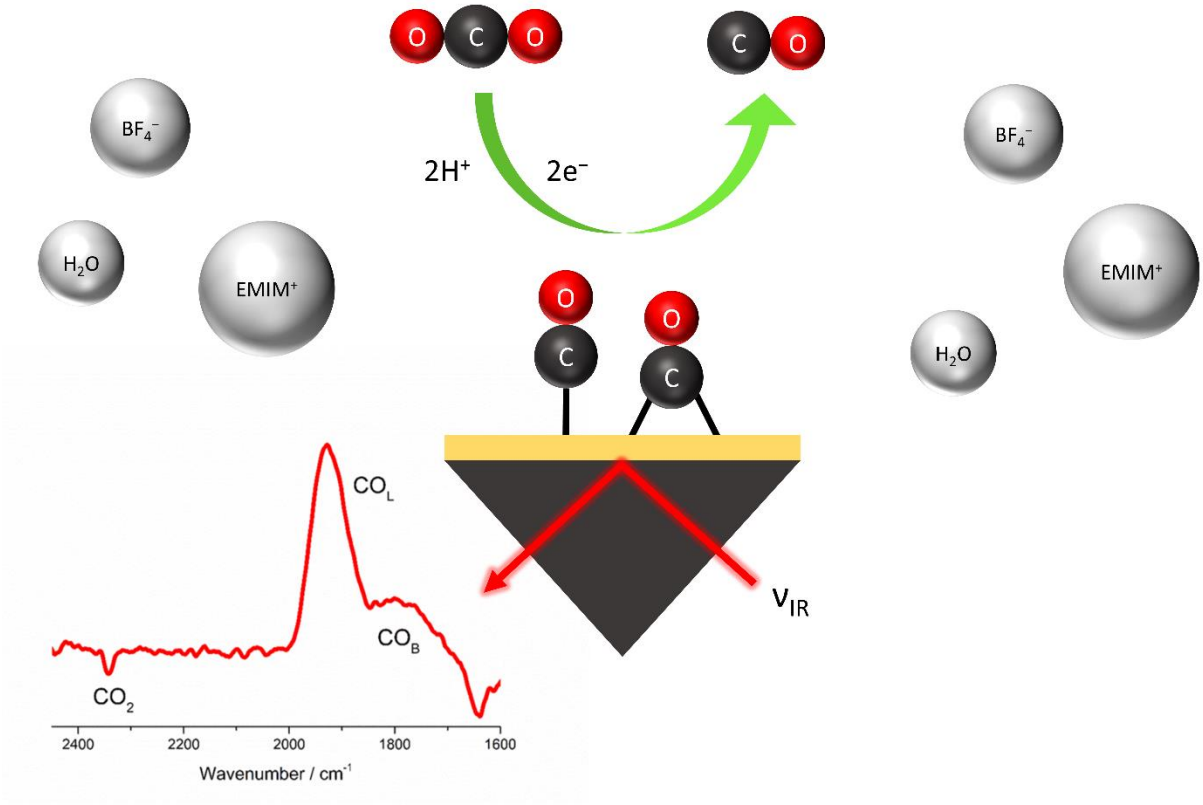
O C O
C O
2H+
2e−
BF4−
H2O
EMIM+
BF4−
EMIM+
H2O
O
C
O
C
VIR
COL
COB
CO2
2400
2200
2000
1800
1600
Wavenumber / cm-1